Supporting Information

High-Performance Magnesium-Ion Thermal Charging Cell Enabled by Organic Cation Pre-Intercalation

Yunjie Xiong, Kang Du, Zongmin Hu and Yimin Xuan*

School of Energy and Power Engineering, Nanjing University of Aeronautics and Astronautics, Nanjing 210016, P.R China
Email address: ymxuan@nuaa.edu.cn

* Corresponding author

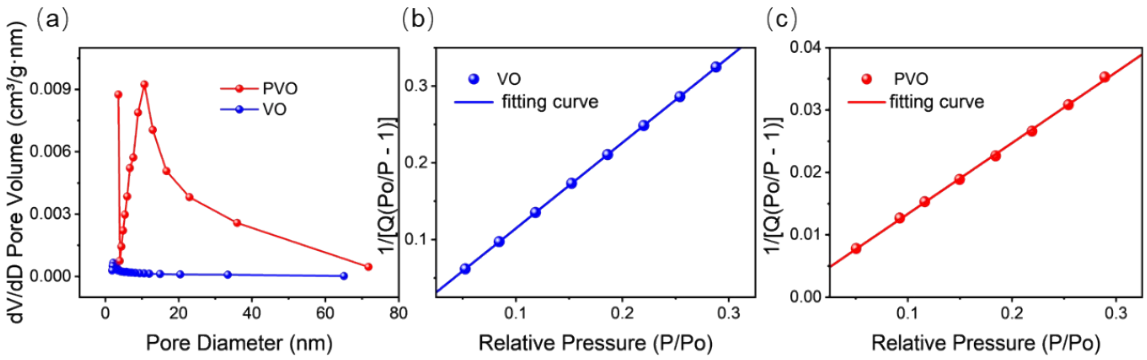

Fig. S1 (a)pore size distribution plots of PVO and VO (b)BET fitting curve of VO (c) BET fitting curve of PVO

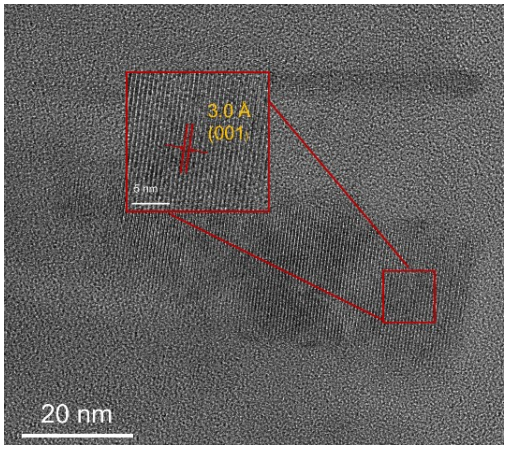

Fig. S2 HRTEM image of VO

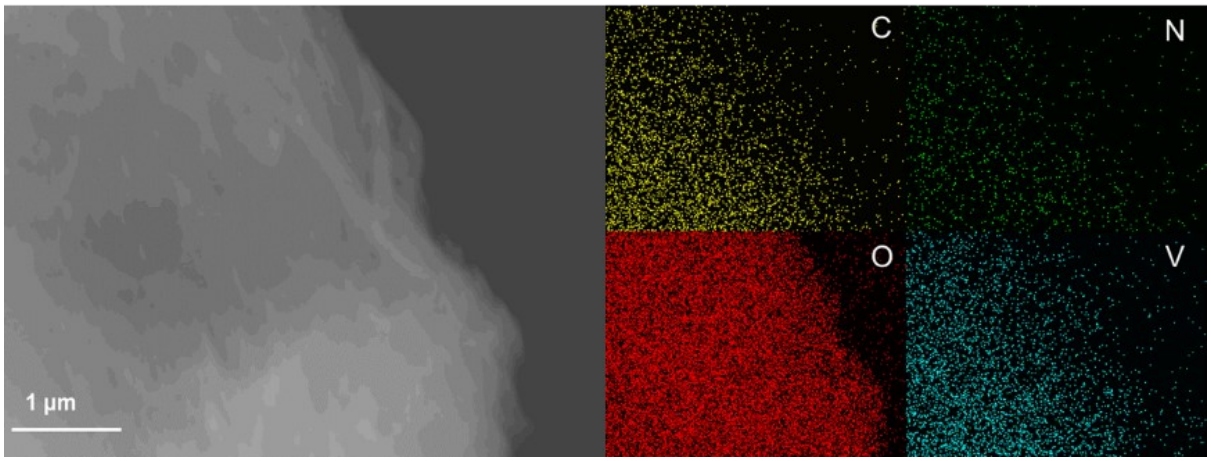

Fig. S3 EDS elemental mapping of PVO.

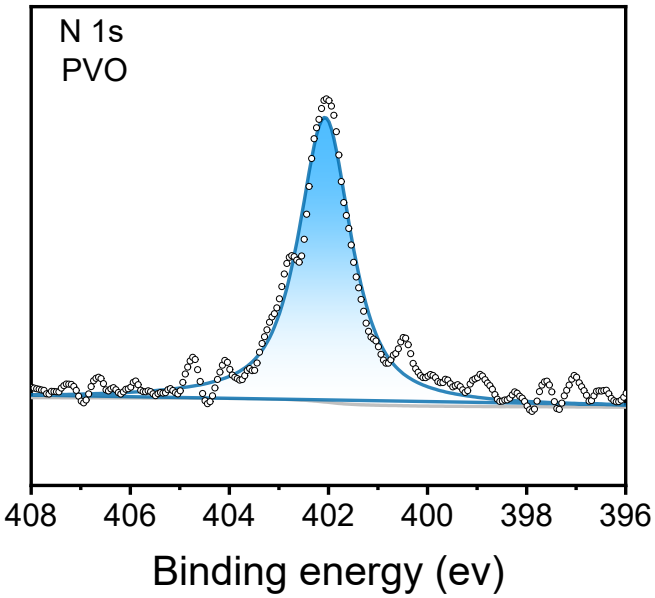

Fig. S4 C1s XPS spectrum of PVO.

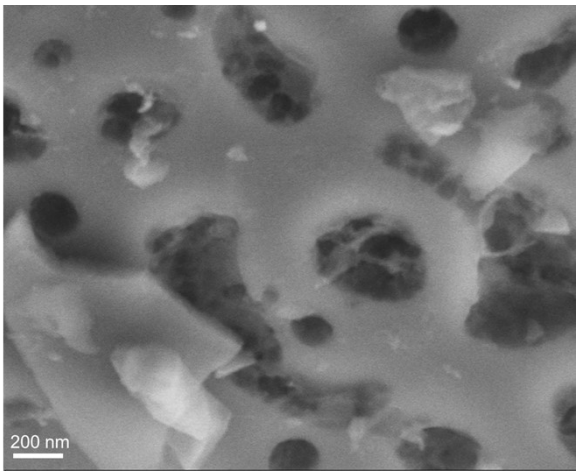

Fig. S5 SEM image of PC.

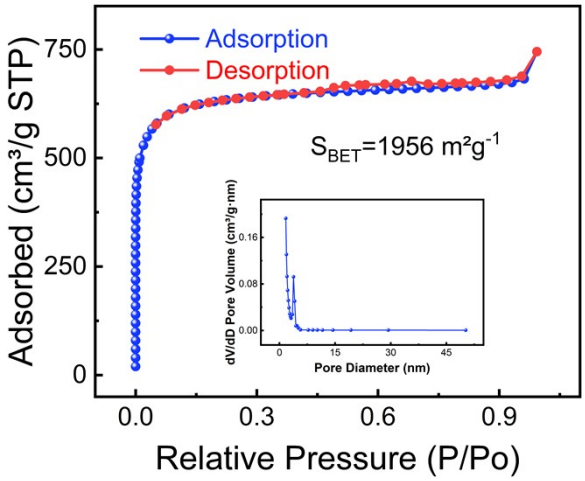

Fig. S6 Nitrogen adsorption-desorption isotherm and the corresponding pore size

distribution of PC.

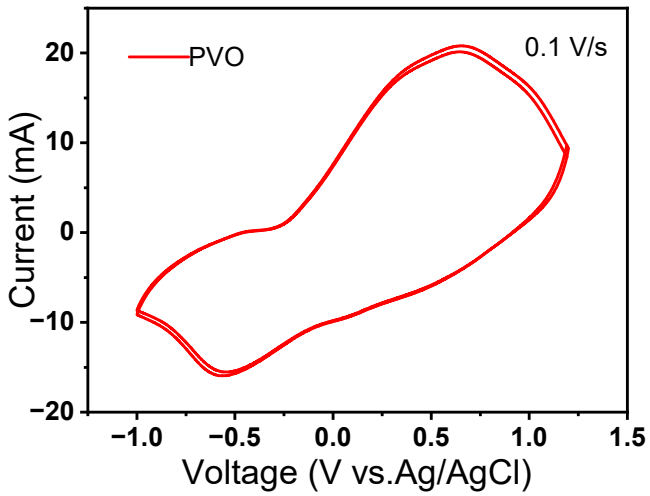

Fig. S7 CV Curves over Multiple Cycles.

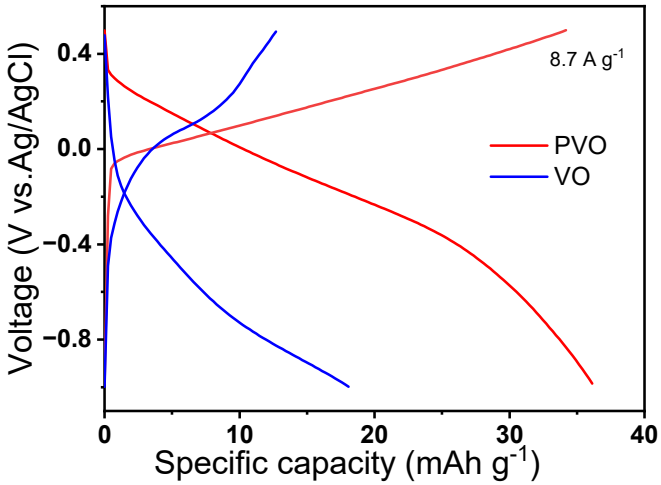

Fig. S8 galvanostatic charge-discharge curves of PVO and VO.

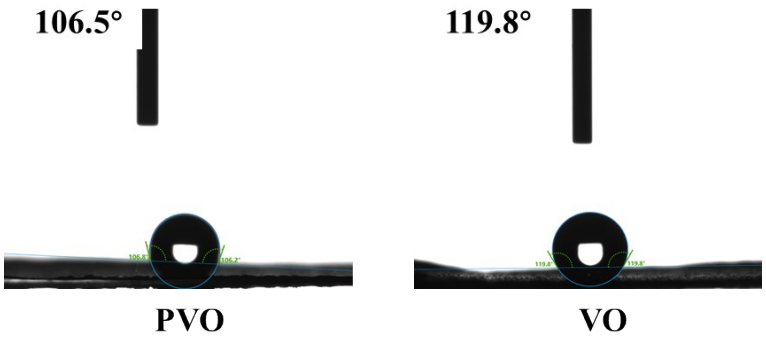

Fig. S9 Contact angle analyses for electrodes of PVO and VO.

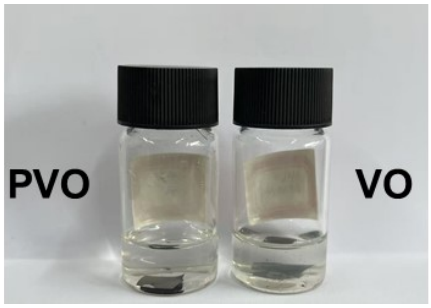

Fig. S10 0.5 M $Mg(CF_3SO_3)_2$ solution after exposing to the different electrodes.

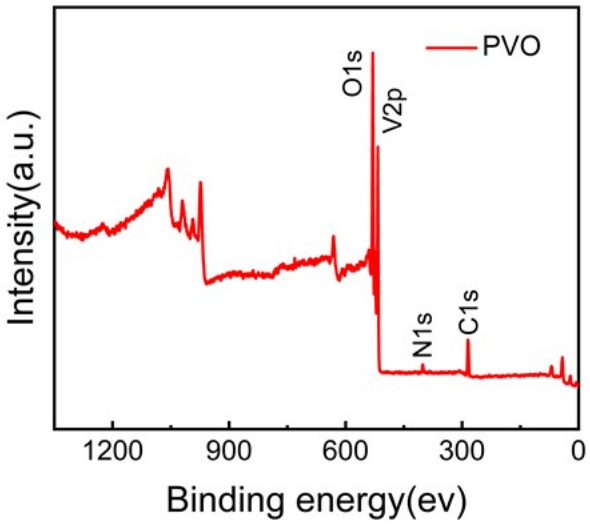

Fig. S11 XPS survey spectrum of pristine PVO electrode

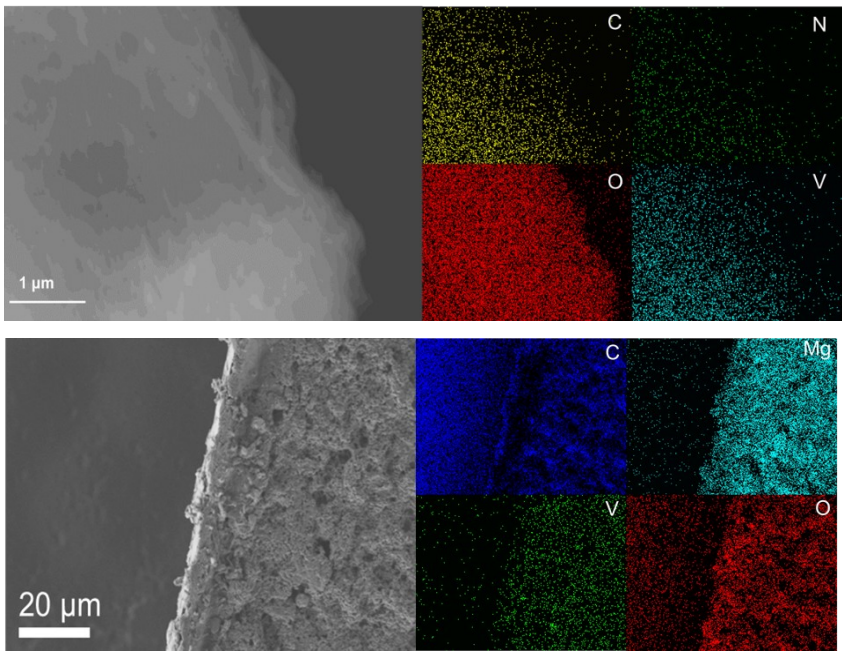

Fig. S12 EDS mapping of pristine and post-hot charged PVO electrode

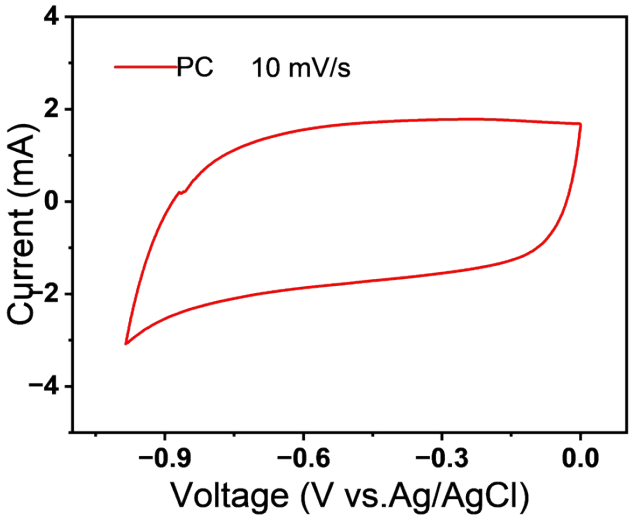

Fig. S13 CV curve of PC electrode

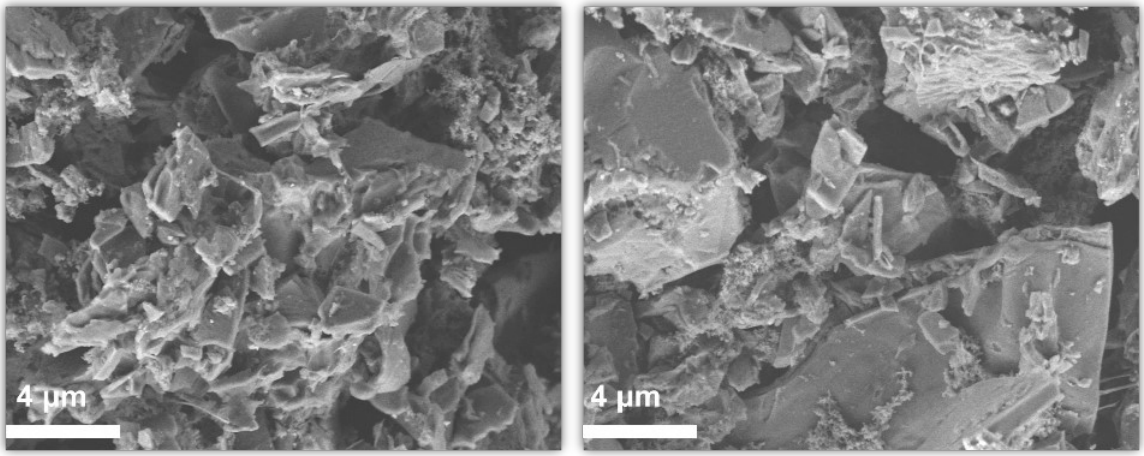

Fig. S14 SEM image of pristine and post-hot charged PC electrode

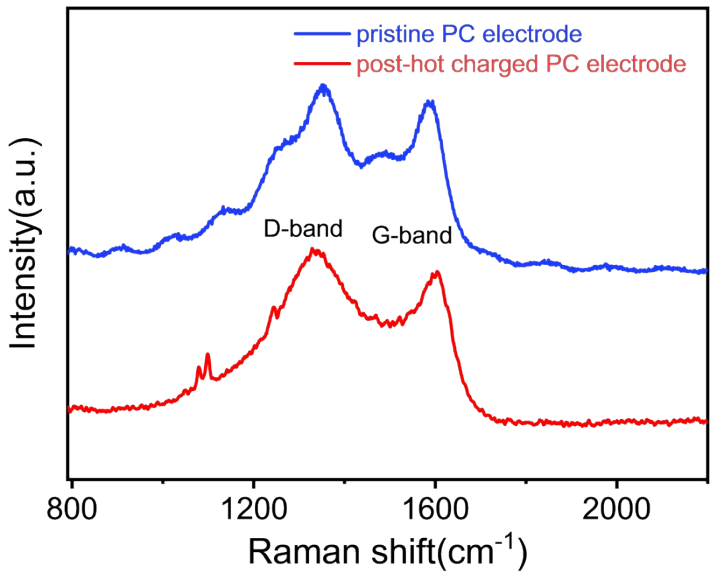

Fig. S15 Raman spectrum of pristine and post-hot charged PC electrode

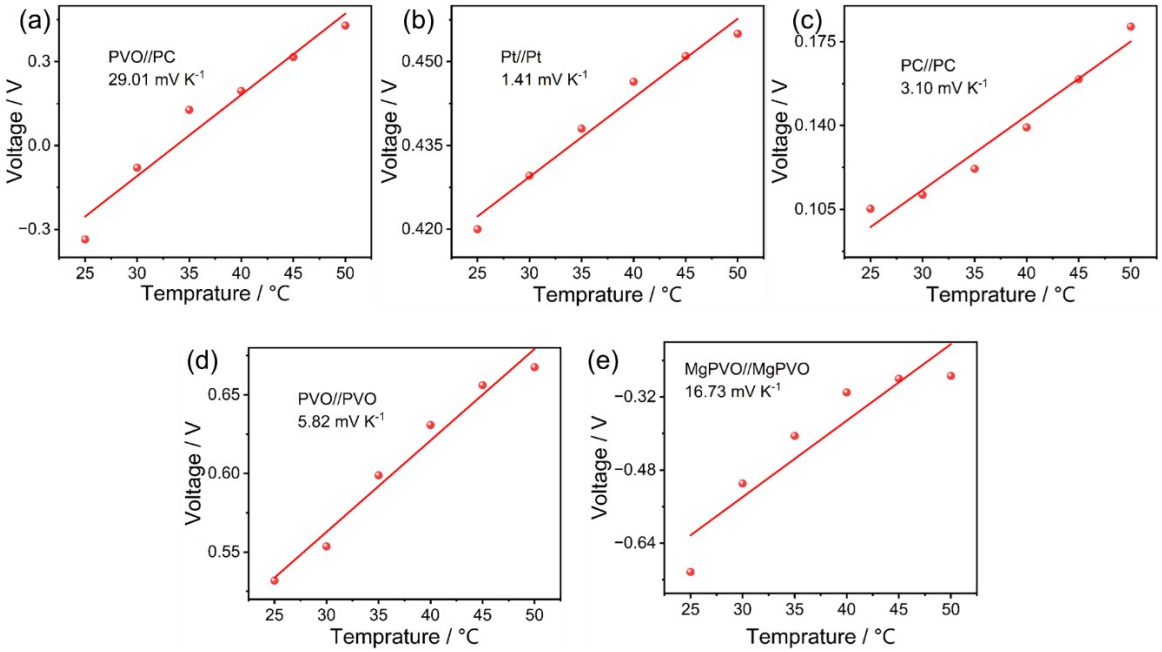

Fig. S16 Temperature dependence of the open-circuit voltage for various systems.

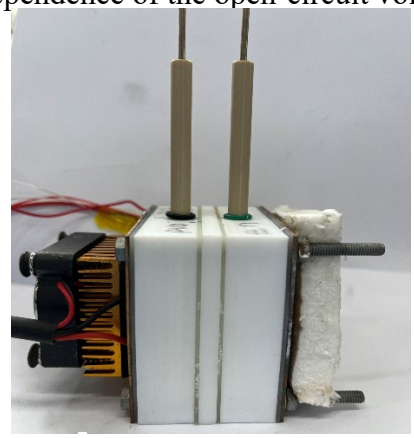

Fig. S17 Photograph of the fabricated planar thermoelectric device.

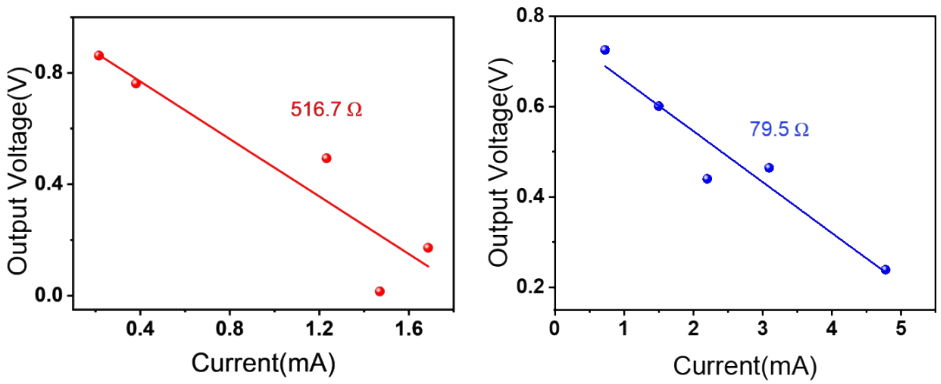

Fig. S18 Fitted impedance plots of various systems.

Table S1 CHNS elemental analysis results of the PVO sample

Sample name	Quality（mg）	N（%）	C（%）	H（%）
PVO	6.780	1.34	9.72	1.84
PVO	6.253	1.33	9.73	1.83

Calculation process of the chemical formula for PVO：The TGA profile indicated negligible mass loss below 200°C, suggesting a minimal water content within the PVO framework. Consequently, a tentative formula was proposed as $[(C_9H_{20}N)x]V_2O_5$ 0.1H2O. To further refine the stoichiometry, CHNS elemental analysis was performed. Among the detected elements, nitrogen (N) was selected as the most reliable indicator for calculating the intercalation degree, as it originates exclusively from the organic cations and remains unaffected by atmospheric moisture or carbon dioxide adsorption, unlike carbon or hydrogen. Based on the measured N content (1.34%), the intercalation coefficient x was determined to be 0.20, yielding the refined formula $[(C_9H_{20}N)_{0.2}]V_2O_5$ $0.1H_2O$. The theoretical mass percentages of C and H derived from this formula were found to be in excellent agreement with the experimental data (Measured C/H: 9.73%/1.84% vs. Theoretical C/H: 10.19%/1.99%), thereby confirming the validity of the proposed stoichiometry.

Table S2 Performance comparision among different systems

Systems	ΔT[a]	$\lvert V_{ovc} \rvert$ [b]	$\lvert \alpha \rvert$ [c]	Ref.
PVO| $Mg(CF_3SO_3)_2$|PC	**40**	**1.196**	**29.9**	**This work**
CVO@OA|Ca(CF_3SO_3)$_2$|PC	45	1.149	25.2	*Energy Storage Mater.* 58, 353–361 (2023)[1]
VO_2-rGO|Zn(CF_3SO_3)$_2$|Zn-G	30	0.7	~23.4	*Nat. Commun.* 14, 6816 (2023).[2]
graphite@Au|gelatin-FeCN4/3- Gr/rGO/GO| graphite@Au	4	0.037	13	*Energy Environ. Sci.* 17, 1559–1569 (2024)[3]
Au/Cu|gelatin- KCl-FeCN4–/3–| Au/Cu	7	0.119	~17	*Adv. Energy Mater.* 12, 2103666 (2022).[4]
nickel sheet|GG-$MA_{4\%}$-gels-$FeCl_{3/2}$| nickel sheet	25	~0.181	7.24	*Energy Environ. Sci.* 17, 1664–1676 (2024)[5]
Porous carbon|Li_2SO_4|Porous carbon	50	0.565	11.1	*ACS Appl. Energy Mater.* 4, 6055–6061 (2021)[6]
CuHCF|$LiNO_3$+KNO_3| LMO	40	0.0464	1.16	*Chem. Mater.* 31, 4379–4384 (2019)[7]
Li|$LiPF_6$-LiTFSI|Li	30	~0.04	1.35	*Nano-Micro Lett.* 16, 72 (2024).[8]
Pt| I_3−/I− EC/DMC|Pt	35	0.27	7.7	*Chem. Eng. J.* 426, 131797 (2021).[9]

[a] Temperature difference (K).

[b] open-circuit voltage(V)

[c]Seebeck coefficient (mV K−1)

Table S3 Parameters for efficiency calculation of MTCC

Seebeck coefficient (mV K^{-1})	29.9
Cold side temperature (K)	303.28
Hot side temperature (K)	343.30
Inter-electrode spacing (m)	0.060
Thermal conductivity (W m^{-1} K^{-1})	0.564
Cross sectional area of the cell (m^2)	0.0001
Inter resistance obtained by voltage-current plot (Ω)	466.99
η_E (%)	2.04
η_{Carnot}(%)	11.66
η_E/η_{Carnot} (%)	17.5

TableS4 detailed definitions of parameters provided of equation* MERGEFORMAT (5)

Symbol	Meaning	Symbol	Meaning
τ	Relaxation time	S	Contact area between electrode and electrolyte
n_m	Molar amount of active material	ΔEs	Voltage drop after current application
V_m	Molar volume of active material	$\Delta E\tau$	Voltage difference (during relaxation process)

1 Z. Hu, S. Chang, C. Cheng, C. Sun, J. Liu, T. Meng, Y. Xuan and M. Ni, *Energy Storage Mater.*, 2023, **58**, 353–361.
2 Z. Li, Y. Xu, L. Wu, J. Cui, H. Dou and X. Zhang, *Nat. Commun.*, 2023, **14**, 6816.
3 C.-G. Han, Y.-B. Zhu, L. Yang, J. Chen, S. Liu, H. Wang, Y. Ma, D. Han and L. Niu, *Energy Environ. Sci.*, 2024, **17**, 1559–1569.
4 Y. Li, Q. Li, X. Zhang, B. Deng, C. Han and W. Liu, *Adv. Energy Mater.*, 2022, **12**, 2103666.
5 J. Hu, J. Wei, J. Li, L. Bai, Y. Liu and Z. Li, *Energy Environ. Sci.*, 2024, **17**, 1664–1676.
6 T. Meng, Y. Xuan and X. Zhang, *ACS Appl. Energy Mater.*, 2021, **4**, 6055–6061.
7 Y. Liu, C. Gao, S. Sim, M. Kim and S. W. Lee, *Chem. Mater.*, 2019, **31**, 4379–4384.
8 Y. Xu, Z. Li, L. Wu, H. Dou and X. Zhang, *Nano-Micro Lett.*, 2024, **16**, 72.
9 K. Kim, J. Kang and H. Lee, *Chem. Eng. J.*, 2021, **426**, 131797.